Sintering of Ceramics

Anne Leriche, Stuart Hampshire, Francis Cambier

Sintering of Ceramics

Anne Leriche, University of Valenciennes and Hainaut-Cambresis, Valenciennes, France
Francis Cambier, Belgian Ceramics Research Centre, Mons, Belgium
Stuart Hampshire, University of Limerick, Limerick, Ireland

1	**Introduction**	1
2	**Thermal Treatment of Ceramics – Sintering**	1
2.1	General Outline	2
2.2	Solid State Sintering	3
2.2.1	Description of matter transport mechanism	3
2.2.2	Grain growth mechanisms	6
2.3	Liquid Phase Sintering	8
2.3.1	Description of matter transport mechanisms	8
2.3.2	Grain growth mechanisms	13
2.4	Densification Kinetics	13
3	**Methods of Controlling Microstructural Development**	14
3.1	Choice of Powder Characteristics	14
3.2	Choice of Optimal Sintering Parameters: Temperature, Time, Heating Rate	14
3.2.1	Controlled rate sintering	14
3.2.2	Fast firing	14
3.2.3	Microwave sintering	14
3.3	Pressure and/or Plasma Assisted Sintering	15
3.3.1	HP	16
3.3.2	HIP	17
3.3.3	SPS	17
3.3.4	Flash sintering	17
3.4	Composition Modification	17
3.4.1	Addition of dopant elements to modify grain boundary energy	17
3.4.2	Addition of extra small particles at grain boundaries	21
3.4.2.1	First example	21
3.4.2.2	Second example	21
4	**Summary**	22
References		23

1 Introduction

Ceramics are inorganic, nonmetallic materials, produced from minerals or synthetic powders which are formed into a shape and consolidated by a high temperature process to densify and strengthen the material and reduce the porosity. Traditional ceramics including pottery and industrial products, such as whitewares, heavy clay-ware and building materials, are formed mainly from natural alumino-silicates and the presence of other minerals including micas and feldspars and some impurities leads to molten viscous phases at the firing temperature. In contrast, advanced ceramics are pure oxides or non-oxides (nitrides, carbides, borides, etc.) or composites of these and include materials that have been developed with designed microstructures for (1) structural applications, making use of their mechanical, tribological or high temperature properties for cutting and drilling tools, bearings, seals, dies, engine components and coatings on other materials to improve corrosion resistance or thermal stability, and (2) functional applications, such as electronic, dielectric and magnetic components, biomedical implants or devices, filters, membranes and catalyst supports.

Most ceramic materials are processed from powders which are shaped and then densified during a heat treatment, where the temperature is sufficiently high, in the range 0.5–0.8 Tm (where Tm is the melting point) to allow diffusion of material. To favor the densification, uniaxial or isostatic external pressure can be applied during thermal treatment (hot pressing (HP) or hot isostatic pressing (HIP) as opposed to pressureless sintering). In addition, an electric current can be used simultaneously with uniaxial pressure (spark plasma sintering (SPS)) or without pressure (flash sintering) or microwave heating can be applied in order to improve the process. In all cases, simultaneously with the densification phenomenon, grain growth can occur which influences the final microstructure. So, it is crucial to know the impact of all process parameters on grain growth and densification mechanisms in order to control the final ceramic microstructure and the resulting properties.

2 Thermal Treatment of Ceramics – Sintering

2.1 General Outline

Owing to the generally high melting points of the raw materials involved, the fabrication of ceramic materials commonly includes a heat treatment in which a powder, already formed into a required shape, is converted into a dense solid. The matter transport to reduce the porosity occurs by diffusion of atoms in the vapor phase, in the liquid phase or in the solid state, or by viscous flow of a glassy phase. Most mechanisms are activated thermally because the action of temperature is necessary to overcome the potential barrier between the initial state of higher energy (porous powder compact) and the final state of lower energy (consolidated dense material) (Hampshire, 2014).

The term sintering is used to refer to all the phenomena occurring during heating, leading to the densification of a powder compact. There are three main types of process for this consolidation to take place and these are dependent on the composition being fired and, in particular, on the extent to which a liquid phase is formed during heat treatment:

1. "Solid state sintering" in the absence of any liquid phase.
2. "Liquid phase sintering" in the presence of a small volume percent of liquid phase.
3. "Viscous flow sintering" when the liquid phase volume is high and similar to the porosity of the powder compact.

In all cases, the driving force for densification lies in the reduction of the surface energy resulting from the reduction in the interfacial area between gas and liquid/solid phases. **Fig. 1** shows a schematic view of the three types of sintering mechanisms.

The green density of the shaped powder compact is usually around 55–60 vol%. This means that full densification of the ceramic will be accompanied by a large amount of shrinkage (decrease of dimensions) of approximately 35–40 vol% and 18–20 linear%. There is also a change in shape of the powder particles with time usually resulting in an increase in average grain size. As shown in **Fig. 2**, the densification rate of a powder compact heated at fixed temperature decreases with time.

The shrinkage of the ceramic compact can be followed at different stages of the process using dilatometry as shown in **Fig. 3**. At the beginning of heating, the sample expands due to increases in the amplitude of thermal vibration of atomic bonds. At higher temperatures, densification commences with reduction of porosity. When the thermal treatment is maintained after complete densification, in some instances, expansion (or dedensification) can occur provoking the appearance of residual porosity and is often associated with initial grain growth.

As shown in **Figs. 2** and **4**, sintering can be presented in three stages:

1. initial stage, during which necks are growing at contact points between particles,

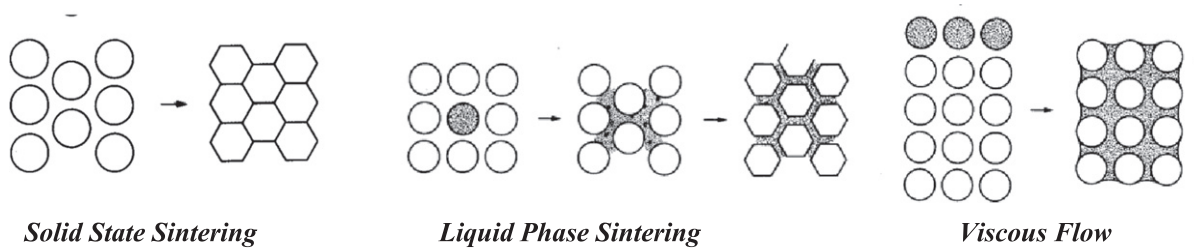

Fig. 1 Sintering mechanisms.

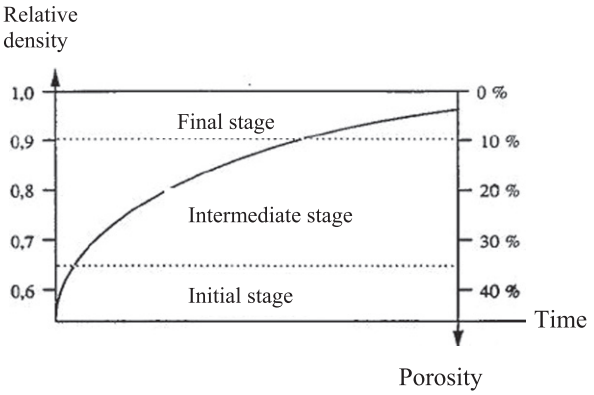

Fig. 2 Schematic curve of densification of a powder compact with time.

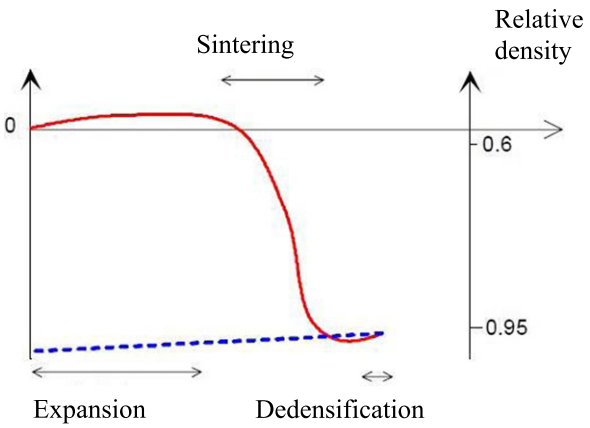

Fig. 3 Classical dilatometric curve.

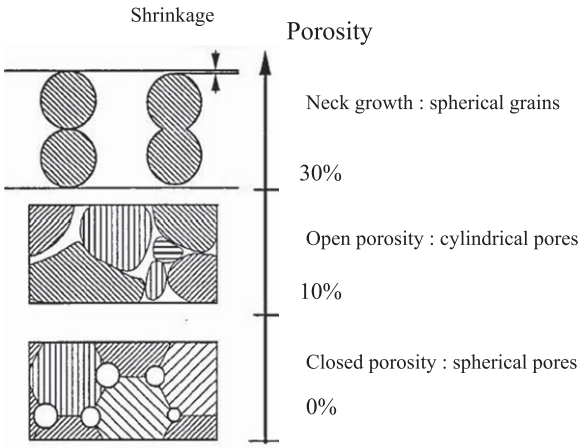

Fig. 4 Grain shape modification during sintering.

2. intermediate stage (65–90% density), during which pores become cylindrically shaped with interconnections, so-called "open porosity,"
3. final stage (90–100% density), during which pores become more spherical and isolated: "closed porosity."

The total interfacial energy of a powder compact is expressed as γA, where γ is the specific surface or interfacial energy and A is the total surface or interfacial area within a powder compact. The reduction in this total energy can be expressed by Kang (2005):

$$\Delta(\gamma A) = \Delta\gamma A + \gamma \Delta A \tag{1}$$

The change in interfacial energy, $\Delta\gamma$, is due to densification and the change in interfacial area, ΔA, occurs because of grain coarsening. $\Delta\gamma$ is related to replacement of solid/vapor interfaces (particle surfaces) by solid/solid interfaces (grain boundaries).

Then, the reduction of total interfacial energy occurs through densification and grain growth (coarsening) as shown schematically in **Fig. 5** (Kang, 2005).

It has been shown that the grain growth becomes predominant during the final stage as illustrated in **Figs. 6** and **7** for sintered titania and alumina powders.

2.2 Solid State Sintering

2.2.1 Description of matter transport mechanism

In solid state sintering, the densification relies wholly on diffusion of atoms (1) at the surface, (2) through the volume, or (3) at grain boundaries with no formation of liquid.

In the absence of liquid phase, the reactions within and between solids require the mobility of atoms and ions. The mechanism of diffusion in solids is the movement of atoms or ions either into vacant lattice sites (vacancies) or between positions that are not normally occupied (interstitial sites).

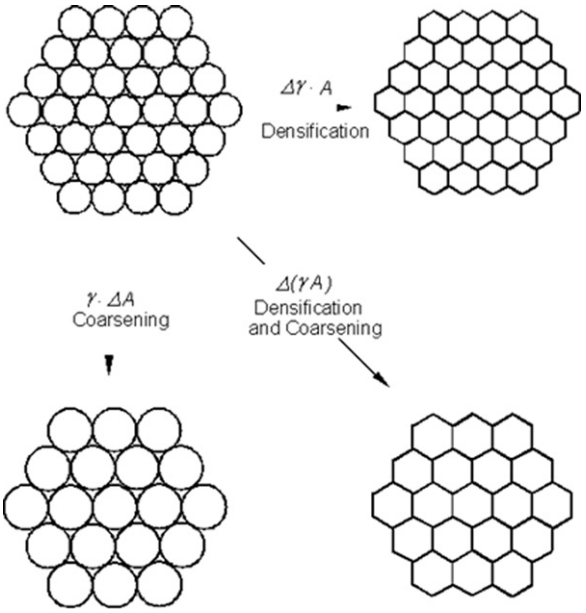

Fig. 5 Basic phenomena (densification and grain coarsening) occurring under the driving force for sintering, $\Delta(\gamma A)$. Reproduced from Kang, S.-J. L., 2005. Sintering, Densification, Grain Growth and Microstructure. Oxford: Elsevier Butterworth-Heinemann.

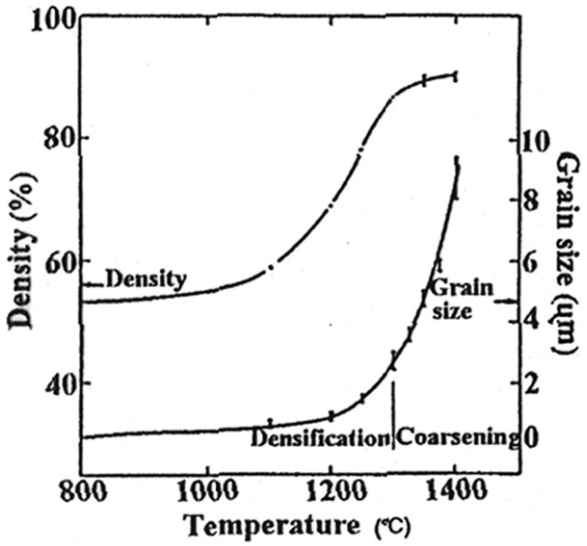

Fig. 6 Density and grain size for powder compact TiO_2 vs. sintering temperature (Rahaman, 1995).

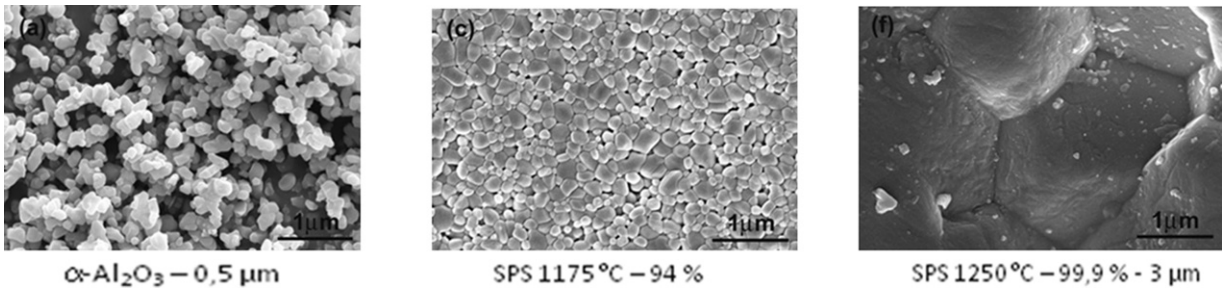

Fig. 7 Microscopic view of alumina powder and resulting microstructure at different densification rates (Reddy *et al.*, 2010).

The driving force for sintering can be described from a macroscopical view as the decrease of free energy by replacement of solid–gas interfaces by solid–solid interfaces and from a microscopical view as the free energy (pressure P) difference across a curved grain boundary. The difference in free energy between the neck area and the surface of the particle provides a driving force which causes the transfer of material by the fastest means available.

The diffusion of atoms occurs in the reverse direction to vacancies which move from areas of higher concentration to ones of lower concentration, that is from concave surfaces to convex surfaces. As presented in **Fig. 8**, the necks between spherical particles are the sink of matter with a diffusion rate as high as the grain curvature ($1/r$) is high (the case of small particles). The driving force P (a few MPa) decreases as sintering progresses, which explains the decrease of densification rate.

$$P = \frac{\alpha\gamma}{r} \tag{2}$$

The matter flux "J" induced by the pressure difference "P" can be expressed by the following Eq. (3) where D is diffusion coefficient, x the transport distance and T the temperature. The value of the diffusion coefficient depends on the transport mechanisms that may operate during solid state sintering of a polycrystalline ceramic and these are shown schematically in **Fig. 9** and are classified below (Kingery *et al.*, 1976).

$$J = -\frac{D}{kT}\frac{\mathrm{d}P}{\mathrm{d}x} \tag{3}$$

Mechanism number	*Transport path*	*Source of matter*	*Sink of matter*
1	Vapor	Surface	Neck
2	Lattice diffusion	Surface	Neck
3	Surface diffusion	Surface	Neck
4	Lattice diffusion	Dislocations	Neck
5	Lattice diffusion	Grain boundary	Neck
6	Boundary diffusion	Grain boundary	Neck

The first three mechanisms with the surface as the source of matter lead to neck growth but no shrinkage and include:

1. Vapor transport D_g: which allows material to be transported from one source surface to another sink surface by evaporation of atoms and condensation at another site, through the pore network. This can also take place because of vapor pressure difference Δp.

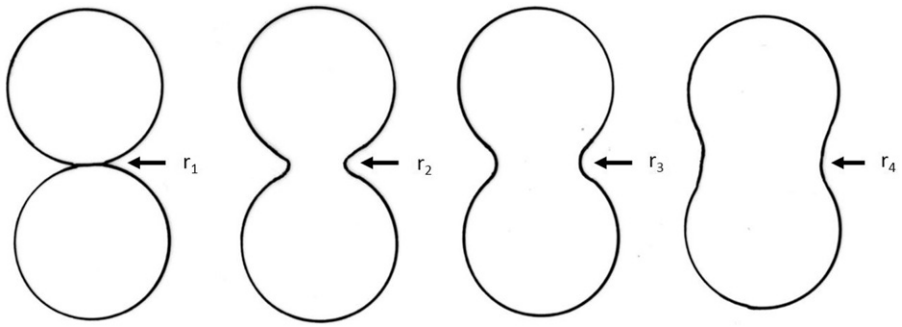

Fig. 8 Shrinkage and shape change of two joined grains.

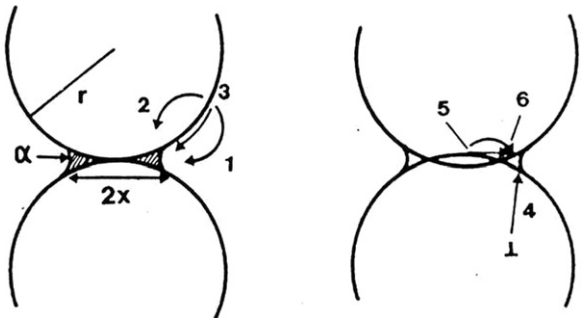

Fig. 9 Transport mechanisms operating during solid state sintering.

2. Lattice diffusion D_l: which allows material to be transported from a particle surface to the neck area by diffusion through the bulk lattice with no increase in densification of the material.
3. Surface diffusion D_s: which involves the diffusion of atoms along surfaces where the source is a particle surface and the sink is a neck. It only occurs to a depth of approximately one to two atomic distances (0.3–0.5 nm) (Rahaman, 2003). This type of diffusion is initiated at lower temperatures due to its lower activation energy and is usually the dominant mass transport mechanism during the early stages of neck growth, as the compact is heated up to the sintering temperature. It becomes less dominant as neck formation between particles increases.

The final three mechanisms with grain boundaries or the bulk material as the source of matter do lead to shrinkage and include:

1. Plastic flow η: which is only active where there is a very high initial dislocation density and therefore is not usually operative in ceramics.
2. Bulk lattice diffusion D_l: which allows atoms from the grain boundary to be transported from the grain boundary through the lattice to a neck or pore surface and so the boundary acts as a site for vacancy annihilation.
3. Grain boundary diffusion D_b: which allows atoms from the grain boundary to be transported along the grain boundary to a neck region or pore surface, driven by the high level of disorientation of the atoms along the grain boundary. Even though grain boundaries are quite narrow they are very active transport paths.

Overall, there is a competition between densification and grain growth and to obtain dense and fine grained ceramics, it is necessary to favor the material transport mechanisms leading to shrinkage and to limit the surface diffusion mechanisms.

The activation energies for surface, grain boundary, and lattice diffusivity increase in that order (Barsoum, 2002) as shown in **Fig. 10** and so the type of matter transport mechanism in operation is highly dependent on the sintering temperature. Thus, surface diffusion is favoured at lower temperature whereas bulk lattice diffusion is favoured at higher temperatures.

$$D_i = D_{0i} e^{-\frac{Q_i}{RT}} \tag{4}$$

The diffusion coefficient is also affected by impurity solutes. In general, the presence of solutes which enhance either boundary or volume diffusion coefficients enhance the rate of solid state sintering. For oxides in which the slowest diffusing species is oxygen, the addition of cations with lower valence state or the use of reducing atmosphere will enhance sintering (e.g., Li_2O in NiO). If the slowest diffusing species is a cation (as for ZrO_2, Y_2O_3, UO_2, etc.), the addition of a higher charged valence state cation will increase the number of host cation vacancies and will thus enhance sintering (e.g., TiO_2 into Y_2O_3). **Fig. 11** presents a typical schematic figure of the microstructure of an oxide and a scanning electron microscopy (SEM) micrograph of a pure oxide (zirconia) after thermal etching. Typically the microstructure of a sintered oxide ceramic consists of equiaxed grains with residual porosity and little or no glassy phase at grain boundaries.

2.2.2 Grain growth mechanisms

The driving force for grain growth is the difference in energy between a fine-grained material and one with a larger grain size resulting from the decrease in grain boundary area and total boundary energy. As the average grain size increases, it is obvious that some grains must shrink and disappear. Due to the free energy difference across a curved grain boundary, the atoms move from a concave to a convex interface and the grain boundary moves toward its center of curvature until the grain disappears as illustrated in **Figs. 12** and **13**.

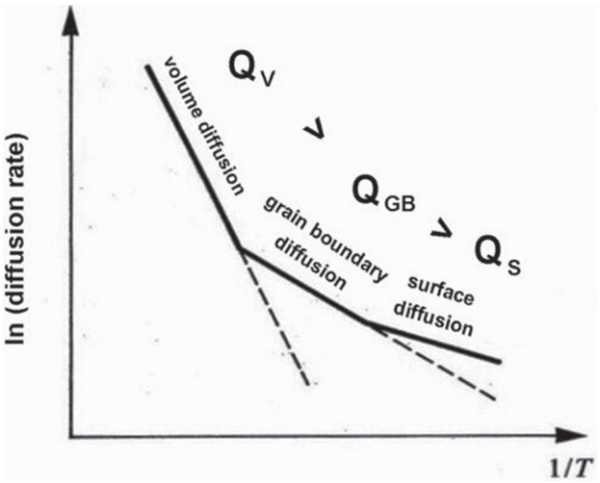

Fig. 10 Temperature dependence of atom diffusion activation energies Q_i.

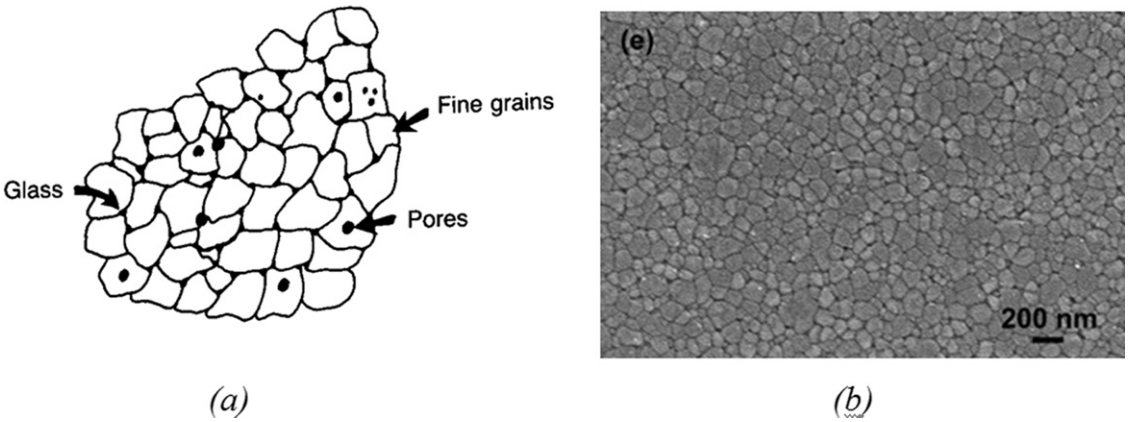

Fig. 11 Typical solid state sintered microstructures (a) schematic (Lee and Rainforth, 1994), (b) scanning electron microscopy (SEM) ZrO_2.

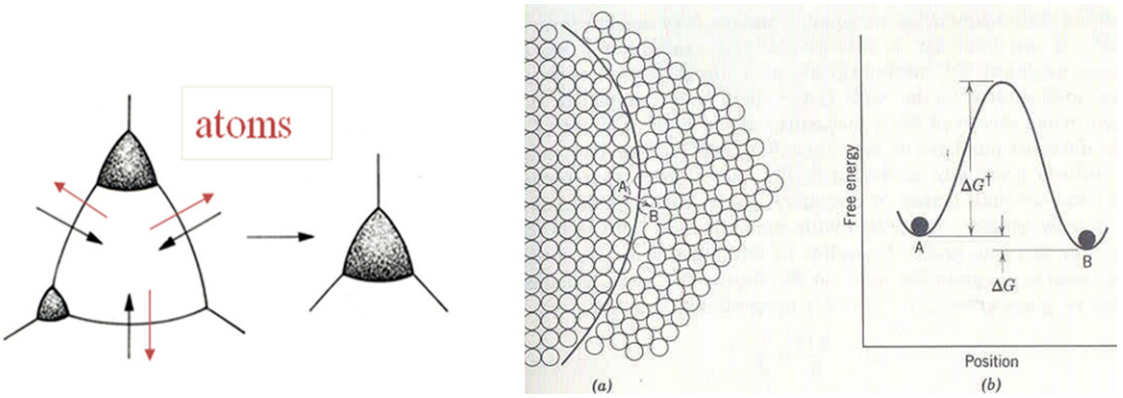

Fig. 12 Disappearance of the grain by atom jumps and pore coalescence (Kingery *et al.*, 1976).

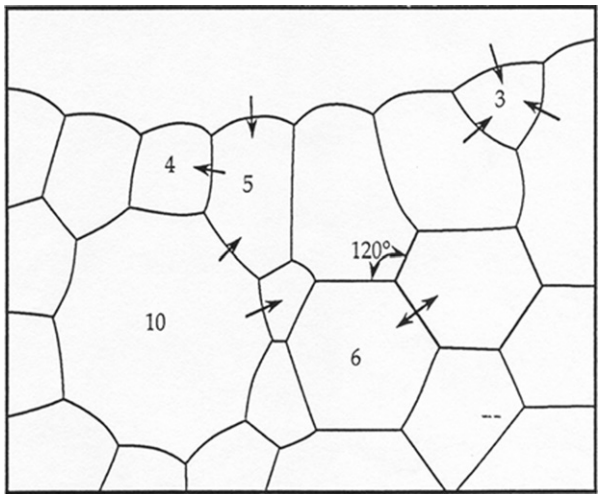

Fig. 13 Grain growth mechanism: arrows indicate the directions in which the boundaries migrate. Small grains (less than six sides) will decrease and finally disappear and the large grains (more than six sides) will increase (Lee and Rainforth, 1994).

The grain growth velocity, v_B, can be estimated from atom flow, J, through a grain boundary:

$$v_B = J\,\Omega \tag{5}$$

$$J = \frac{D_b}{kT}\frac{\Delta P}{dx} = \frac{-D_b}{kT}\frac{\alpha\gamma}{r}\frac{1}{\delta_b} \tag{6}$$

$$\frac{\mathrm{d}(GG)}{\mathrm{d}t} \sim d^{-2} \tag{7}$$

where Ω is atomic volume and δ_b the grain boundary thickness.

Simultaneously with normal grain growth, exaggerated grain growth (EGG) can occur as illustrated in **Figs. 14** and **15**. This phenomenon can be avoided by addition of dopants which segregate at grain boundaries (e.g., ~300 ppm MgO in alumina).

Simultaneously with grain growth, pore shape distortion can occur from a spherical shape by the moving boundary and pore agglomeration. The stability of a pore depends on both the dihedral angle and the number of surrounding grains which gives N_c, the critical number of grains surrounding a pore as shown in **Figs. 16** and **17**. When the number of surrounding grains is higher than N_c for a given dihedral angle, the pore size increases and it decreases when the number of surrounding grains is lower (**Fig. 18**).

The pore stability conditions change with pore size as shown in **Fig. 19**. The larger is the pore, the greater will be the dihedral angle to eliminate the pore.

When grain growth occurs, many pores become isolated from the grain boundaries and the diffusion distance between pores and a grain boundary becomes large, and the rate of sintering decreases. The most satisfactory way of obtaining densification is to prevent or to slow boundary migration by various methods which are described in Section 3.

2.3 Liquid Phase Sintering

2.3.1 Description of matter transport mechanisms

Contrary to sintering by viscous flow, the liquid volume formed by the partial melting of one or more components has to be limited to a small volume fraction in order to keep the compact shape and to limit the amount of glassy/amorphous phase in the final product. It is represented in **Fig. 20** as a thin liquid layer around each particle. The matter transport occurs by atom diffusion through the superficial liquid phase (D_l).

$$J = -\frac{D_l}{kT}\frac{\mathrm{d}P}{\mathrm{d}x} \tag{8}$$

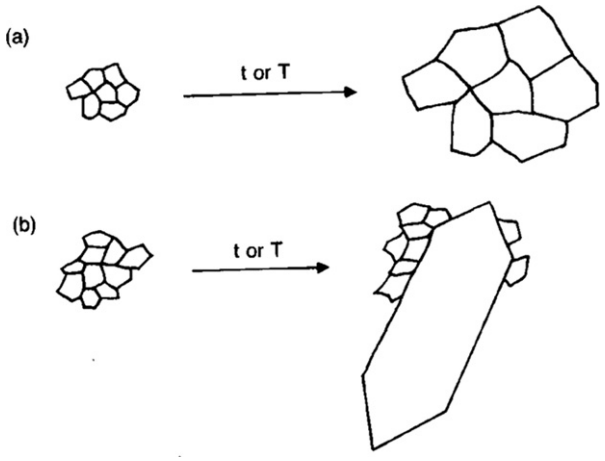

Fig. 14 Grain growth phenomena: (a) normal grain growth and (b) exaggerated grain growth (EGG).

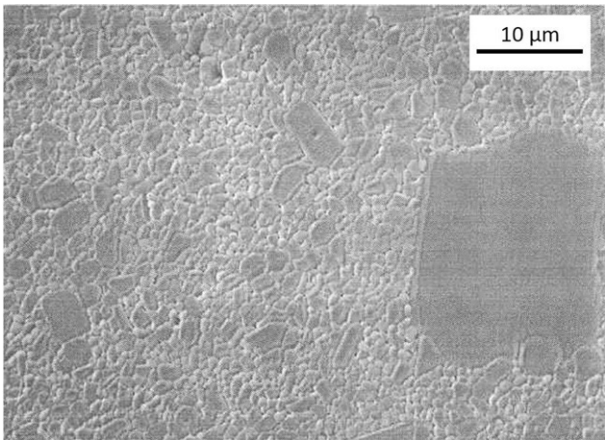

Fig. 15 Microstructure of alumina with exaggerated grain growth (EGG).

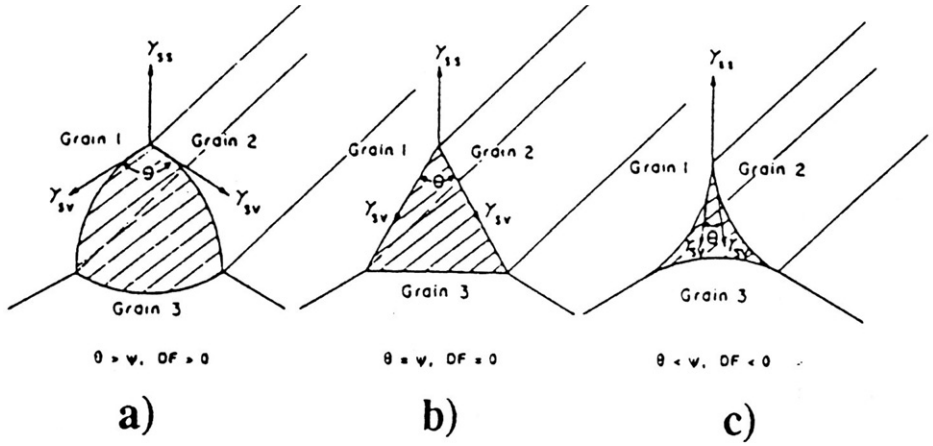

Fig. 16 Conditions for pore stability vs. dihedral angle. (a) Pore shrinkage, (b) pore stability, and (c) pore growth.

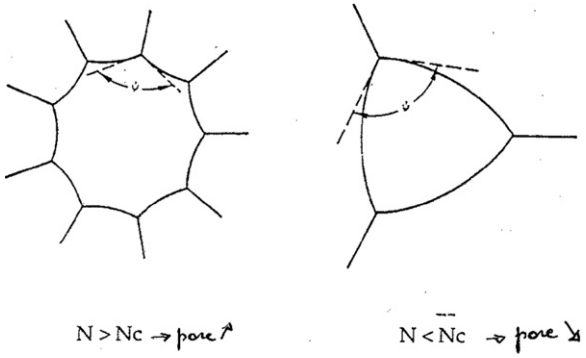

Fig. 17 Conditions for pore stability vs. surrounding grain number.

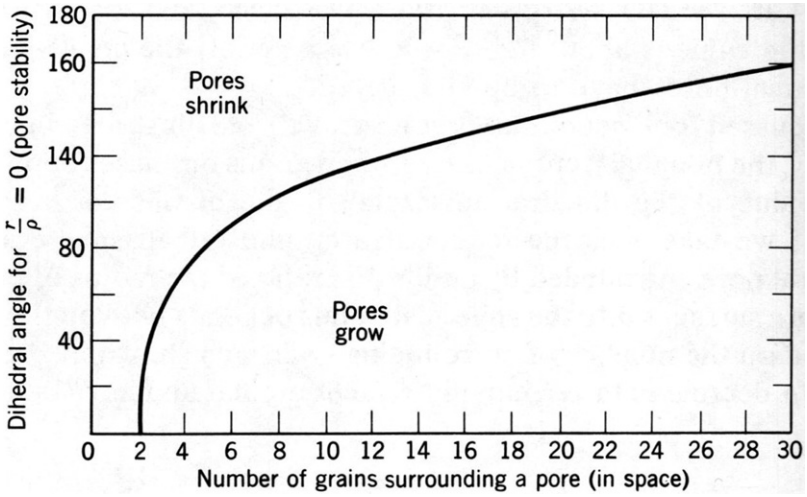

Fig. 18 Conditions for pore stability (Kingery *et al.*, 1976).

Therefore, the parameters which control densification include grain size and shape, pore size and shape, liquid volume and viscosity, solubility of the solid, wetting of the solid by the liquid, phase distribution and phase-boundary energies.

Consider a drop of liquid resting on the surface of a solid phase, as in **Fig. 21(a)**, the system will reach equilibrium such that:

$$\gamma_{SV} - \gamma_{SL} = \gamma_{LV} \cos\theta \tag{9}$$

where γ is the surface energy of the respective interfaces (SV – solid/vapor; SL – solid/liquid; LV – liquid/vapor).

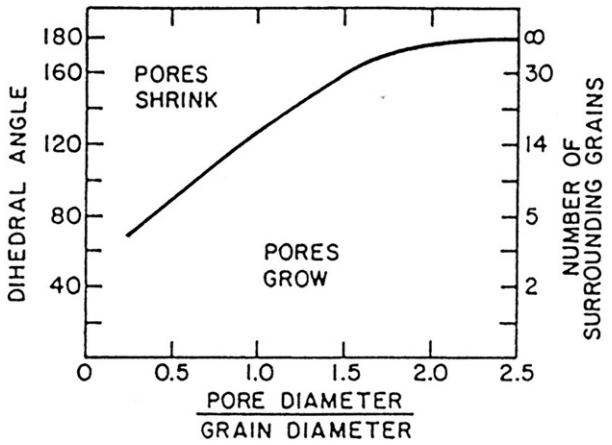

Fig. 19 Pore stability vs. pore size (Ewsuk and Messing, 1989).

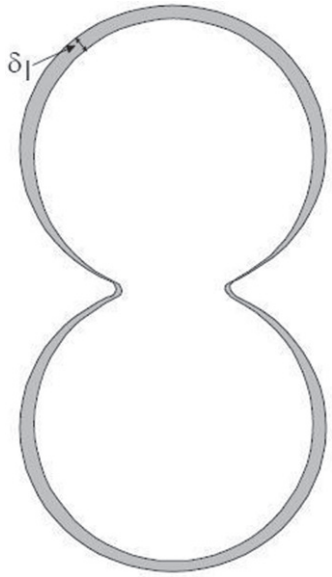

Fig. 20 Superficial liquid phase on two spherical particles.

If $\theta < 90$ degree, then the liquid wets the solid.

If $\theta = 0$ degree, the liquid will spread along the solid surface but complete wetting cannot occur if $\gamma_{LV} > \gamma_{SV}$.

If the liquid is surrounded by the solid as in a pore, the conditions are slightly different because spreading generates only new liquid–solid interface but no new liquid–vapor interface. A wetting liquid will always tend to rise up a capillary or be drawn into a pore, even if it would not spread on a free surface. Where the liquid phase is in contact with a solid grain boundary as in **Fig. 21(b)**, penetration of the liquid between the grains will be dependent on the surface energies involved.

At equilibrium:

$$\gamma_{GB} = 2\gamma_{SL} \cos(\phi/2) \tag{10}$$

where ϕ is the dihedral angle. In the case of complete wetting, the liquid phase can penetrate along the grain boundaries and separate the grains.

To be efficient, the liquid phase should wet the grains and penetrate along the grain boundary. For this to occur, the dihedral angle must be less than 60 degree as shown in **Fig. 22**.

Jackson *et al.* (1963) showed that increasing the dihedral angle and the degree of solid–solid contact between grains tends to increase the resistance to shrinkage and densification. This occurs mainly during the initial rapid formation of the liquid phase when any grain-to-grain contact inhibits the ability of the particles to rearrange within the liquid phase.

The driving force for densification is derived from this capillary pressure of the liquid phase located between the fine solid particles. Each interparticle space becomes a capillary in which capillary pressure is developed. For submicron particle sizes, capillaries with diameters in the range of 0.1–1 μm develop pressures in the range of 1.25–12.5 MPa.

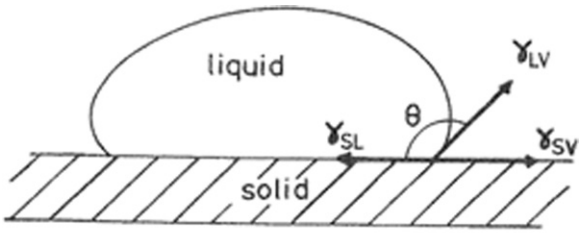

(a)

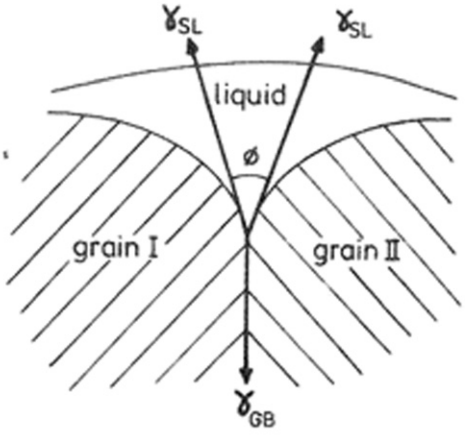

(b)

Fig. 21 (a) Liquid drop on solid substrate showing contact angle, θ; (b) liquid penetration along grain boundary depends on dihedral angle, ϕ. (Smith, 1948).

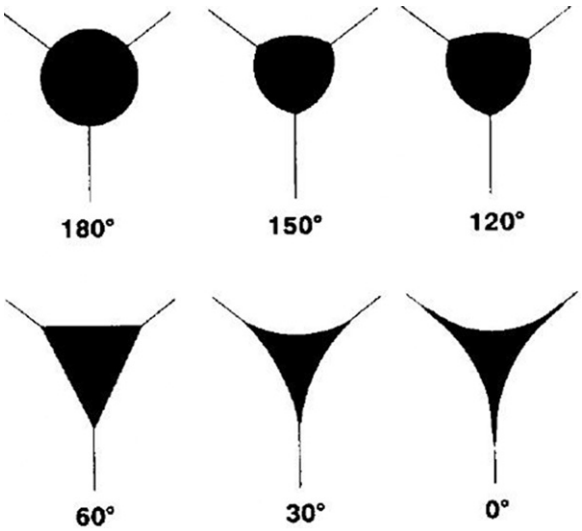

Fig. 22 Penetration of the liquid between the grains as a function of the contact angle.

The presence of liquid and the capillary pressure result in densification via three distinct stages (Kingery, 1959):

1. Particle rearrangement stage.
2. Solution-diffusion-precipitation stage.
3. Coalescence stage.

During the first stage, the liquid which is first formed is drawn by capillary forces to the points of contact between grains at a rate which is determined by the surface tension and viscosity of the liquid. Particle rearrangement thus occurs by viscous flow. The proportion of complete densification that can be achieved through a rearrangement process with spherical particles depends on the volume fraction of liquid present (Fig. 23).

The shrinkage may also depend on particle shape and size distribution, the solubility of the solid in the liquid and interfacial energies.

The second stage involves atom transport in the liquid by solution, diffusion and reprecipitation and proceeds in three steps: (1) atom migration to the grain surface followed by interfacial reaction leading to dissolution of solid in the liquid phase; (2) matter transport by diffusion through the liquid to points away from the contact areas; and finally (3) the reprecipitation of solid material either at grain boundaries or on existing seed crystals (e.g., in silicon nitride, where initially α-silicon nitride is dissolved and β-silicon nitride precipitates on existing β seeds).

For very small crystals, the interfacial tensions between the crystals and their saturated solution is greater than that for large crystals. According to the Gibbs–Thompson equation, the solubility of small grains is larger than large grains.

$$\log\frac{S_r}{S} = \frac{2\,M\gamma}{N_0 kT\rho\, r} \tag{11}$$

where S_r and S are the solubilities of particles with radius r or infinite radius, M is the molar mass, γ is the surface energy, N_0 is Avagadro's number, k is Boltzmann's constant, T is the absolute temperature, ρ is the particle density, and r is the grain curvature radius.

The third stage of sintering involves a reduction in the densification rate which may be caused by a number of different processes including (1) grain growth which prevents further transport of liquid phase, (2) trapping of gases in closed pores with the resulting pressure acting against the capillary pressure normally causing shrinkage, etc.

Successful systems require sufficient liquid volume, a good wettability of the powder particles by the liquid and partial solubility of the solid in the liquid.

Fig. 24 shows typical examples of microstructures: (a) mullite–zirconia composites synthesized by reaction sintering from zirconium silicate and alumina and (b) silicon nitride with MgO/Y_2O_3 as sintering additives. The chemically etched

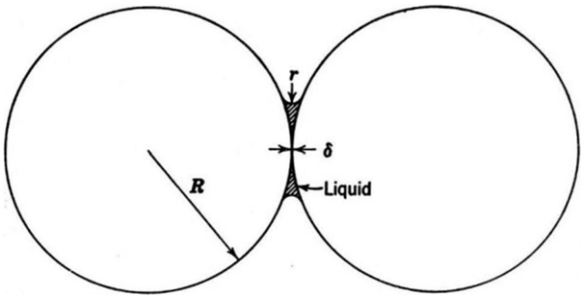

Fig. 23 Liquid is drawn by capillary forces to the points of contact between grains (Kingery, 1959).

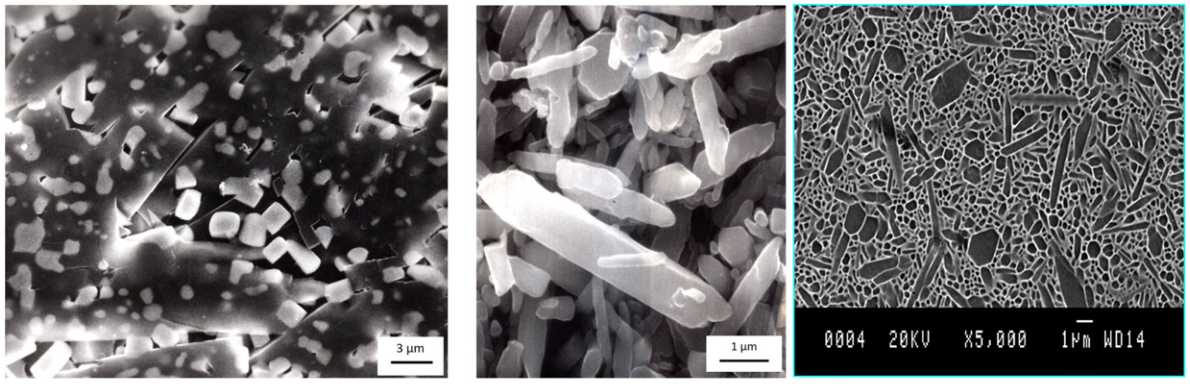

Fig. 24 Some typical microstructures of liquid phase sintered ceramics: (a) reaction-sintered mullite–zirconia (Leriche, 1986) and (b) sintered silicon nitride (left: grain morphology, right: 2D section showing elongated grains surrounded by secondary glass phase (Hampshire and Pomeroy, 2012).

microstructures show needle-like elongated grains of mullite or silicon nitride. The glassy phase formed by cooling from the liquid phase is located at grain boundaries.

2.3.2 Grain growth mechanisms

For liquid phase sintering, the grain growth can be controlled either by the dissolution step or by the diffusion step.

In the case of the rate control by diffusion, the grain growth follows the relationship:

$$d^3 - d_0^3 = k_1 t \tag{12}$$

where d_0 is initial grain size and k_1 is a constant depending on D_L, Ω, C, γ_{SL}, k, and T.

A similar dependence exists for a model described by Raj and Chyung (1980) for the creep of materials containing an intergranular liquid phase

$$\frac{d\varepsilon}{dt} = \frac{3.7\sigma\Omega C\alpha}{(1-x)\eta d^3} \tag{13}$$

where ε is the strain, σ is the applied stress, η is the viscosity of the liquid, C is the molar content of solute in the liquid phase and x is the amount of liquid. This relationship has the advantage of showing the influence of liquid viscosity on diffusion rate.

If the grain growth is controlled by the interfacial reaction (as occurs in the case of a low viscosity liquid), the phenomenon can be described by the relationships in Eq. (14) giving square of grain size, d^2, dependence and the liquid phase viscosity does not affect the grain growth rate.

$$d^2 - d_0^2 = k_2 t \qquad k_2 = \frac{256C\Omega\gamma_{SL}k_R}{81kT} \tag{14}$$

where k_2 is a constant depending on Ω, C, γ_{SL}, k_R (the atom transfer rate between crystal and liquid), k, T.

The comparison with the creep rate model for dissolution reaction gives a different dependence with grain size:

$$\frac{d\varepsilon}{dt} = \frac{\sigma\Omega K'}{2(1-x)kTd} \tag{15}$$

where x is the surface volume fraction occupied by the liquid at the grain boundary.

2.4 Densification Kinetics

Kuczynski (1949) analysed the rate of growth of the neck during the initial stage for various mechanisms of transport of material into the neck from the particle surface and Herring (1951) included the effects of particle size. For all mechanisms, a general relationship follows:

$$(x/r)^n = K_1 t/r^m \tag{16}$$

where r is the particle radius, x is the radius of the interparticle contact area, t is the time and n, m, and K_1 are constants. Plots of log (x/r) versus log t or log r should result in linear plots with slopes of n or m.

During the second intermediate stage, depending on the mechanism of material transport, shrinkage may occur according to:

$$\Delta L/L_o = K_2 t^{\gamma} \tag{17}$$

where ΔL is change in length, L_o is the original length, t is the time and γ and K_2 are constants. A plot of $\Delta L/L_o$ versus log t should be linear with slope γ.

The mechanism of material transport is then deduced from the slope as follows:

	n	m	γ
Surface diffusion D_s	7	4	No shrinkage
Evaporation/condensation D_g	3	2	No shrinkage
Volume (bulk) diffusion D_l	5	3	0.4/0.5
Grain boundary diffusion D_B	5	3	0.3/0.33
Viscous/plastic flow η	2	1	1

Particle size, packing, degree of agglomeration, presence of impurities, sintering atmosphere, etc. can affect the mechanism of sintering, the extent of pore/grain boundary interactions (Brook, 1969) and whether densification or coarsening occurs.

Fig. 25 shows schematic curves of relative density versus time and the effects of temperature, pressure and particle size.

Increase in temperature favors atomic diffusion through the Arrhenius relationship, external pressure will increase the sintering driving force (γ/r) and decrease in grain size decreases the diffusion distance. For an identical particle size, a temperature increase favors successively D_S, D_b, and D_L. So, low temperature sintering favouring D_S (neck growth without shrinkage) will be chosen to process porous materials whereas achievement of high densities will require high temperature sintering to favor D_L (shrinkage).

The following section outlines the different ways of achieving high densification rates by limiting grain growth during sintering.

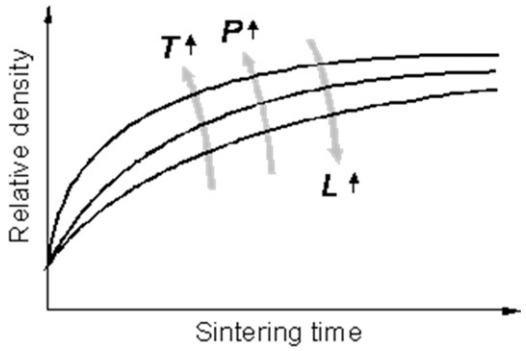

Fig. 25 Effect of sintering parameters (T – Temperature, P – Pressure, L – particle size) on densification. Reproduced from Kang, S.-J.L., 2005. Sintering, Densification, Grain Growth and Microstructure. Oxford: Elsevier Butterworth-Heinemann.

3 Methods of Controlling Microstructural Development

Microstructure can be controlled by optimization of the fabrication process through careful choice of raw materials, selection of the appropriate shaping technology and optimization of the temperature – time schedule during sintering. In addition, the thermal treatment can be modified, particularly using pressure assisted methods such as HP, HIP, post-sintering HIP treatments, where the driving force includes an extra parameter related to external pressure ($2\gamma/r + P_{ext}$), and methods such as SPS and flash sintering where the application of an electrical field induces increases in densification rates.

3.1 Choice of Powder Characteristics

It should be noted that the most important parameter influencing densification and grain growth is the powder characteristics and in particular its mean size and grain size distribution. Thus, narrow grain size distribution (Ø max/Ø medium ≤ 2) is preferable for a high density. This was experimentally confirmed for a submicron TiO_2 powder which can be fully sintered at 300K below the temperature normally required for a powder with the usual grain size distribution (Haussonne *et al.*, 2005).

3.2 Choice of Optimal Sintering Parameters: Temperature, Time, Heating Rate

In the previous paragraphs, it was explained that temperature favors the densification rate but also that the concurrent grain growth phenomenon becomes predominant at the final stage of densification. A close control of the temperature cycle is therefore needed to obtain the optimum microstructure. Several sintering methods are based on heating rate control.

3.2.1 Controlled rate sintering

This technique was proposed by Palmour and Johnson (1967) and Palmour *et al.* (1977). It allows optimization of grain size and pore elimination by maintaining a constant densification rate at relative densities >0.75 to favor grain boundary diffusion, D_b, rather than surface diffusion, D_S (**Fig. 26**).

The objectives of the following methods are to heat a powder compact at much higher heating rates than in conventional sintering in order to reduce the dwell time during the low temperature range which favors densification with minimal grain growth.

3.2.2 Fast firing

Fast firing (Harmer and Brook, 1981) was proposed as a sintering method in order to enhance densification and suppress grain growth and consists of the introduction of green samples rapidly into the hot zone of a furnace so that the samples attain higher temperatures very rapidly where the activation energy for densification, Q_ρ, is higher than Q_g, the activation energy for grain growth as shown in **Fig. 27**. Fast firing thus allows a powder compact to reach temperatures above T_{int} very quickly thus minimizing grain coarsening during heating.

Unfortunately, this technique has to be restricted to small size samples because of the large thermal gradients generated by fast heating and cooling. For instance, small disks of barium titanate capacitors are sintered by this method.

3.2.3 Microwave sintering

Microwave sintering allows reductions in both sintering temperature and time as there is direct coupling of the microwaves with electric dipoles within the ceramic (Binner and Vaidhyanathan, 2008). This is thought to be due to the higher heating rate which brings the ceramic up to the sintering temperature more rapidly so avoiding the lower temperature region where the rate of grain growth is higher than the rate of densification. Full density can be achieved within a few minutes at several hundred degrees below the conventional sintering temperature (**Fig. 28**).

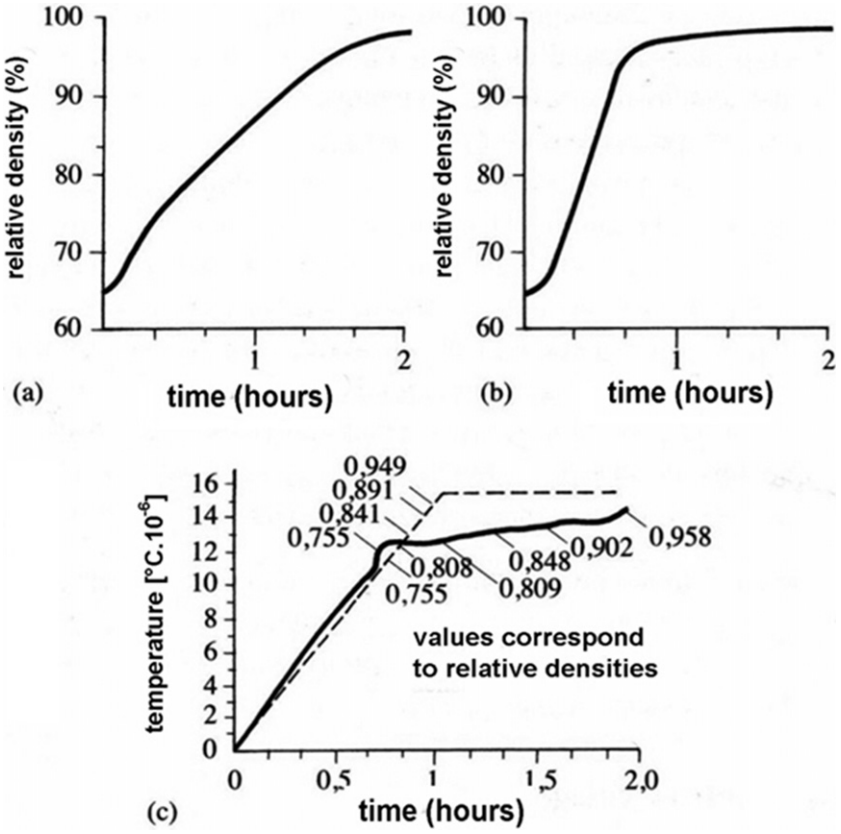

Fig. 26 (a) Rate-controlled density–time curve suggested by Palmour and Johnson (1967) and Palmour *et al.* (1977), (b) conventional density–time curve, (c) temperature–time dependence with relative densities (Haussonne *et al.*, 2005).

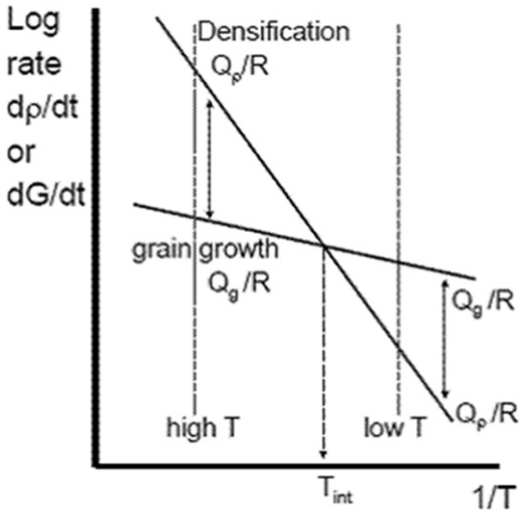

Fig. 27 Densification rate or grain growth rate as a function of temperature. Adapted from Harmer, M.P., Brook, R.J., 1981. Fast firing – Microstructural benefits. Transactions and Journal of the British Ceramic Society 80, 147–149.

3.3 Pressure and/or Plasma Assisted Sintering

Densification of ceramics can be achieved more effectively using pressure-assisted forming techniques which combine external pressure with temperature in order to enhance the final density. These include HP, HIP, sinter forging, hot extrusion, and gas pressure sintering. More recently, electrical field assisted sintering techniques (FAST) have been developed.

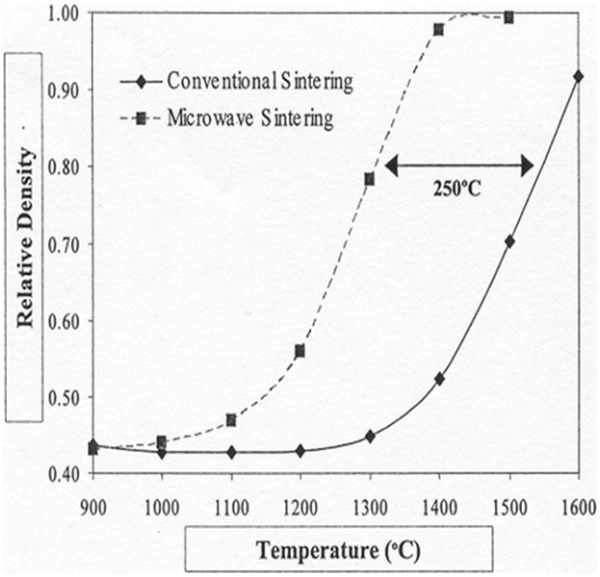

Fig. 28 Decrease of sintering temperature for microwave sintering for alumina (Brosnan *et al.*, 2003).

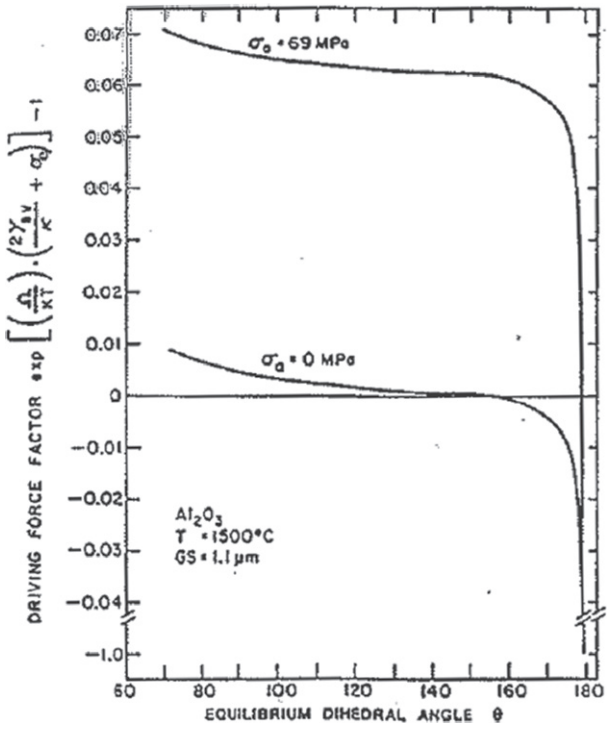

Fig. 29 Densification driving force factor vs. dihedral angle for pressureless sintering and hot isostatic pressing (HIP) (Ewsuk and Messing, 1989).

The application of an external pressure (σ_a) allows the acceleration of densification but also modifies the pore stability conditions as shown in **Fig. 29** which allows to eliminate pores which by pressureless sintering would be stable or would have grown.

$$\mathrm{DF} = \frac{2\gamma}{\kappa} + \sigma_a \quad \text{with} \quad \kappa = r\frac{\sin\left(90 - \frac{\psi}{2}\right)}{\sin\left(\frac{\theta}{2} - \frac{\psi}{2}\right)} \tag{18}$$

3.3.1 HP

This technique involves application of a uniaxial pressure through a simple shaped die and only produces simple shaped components which require subsequent diamond machining to final tolerances. The use of applied pressure (10–30 MPa) at the

sintering temperature increases the densification rate and the ability to reach near-theoretical density in a reasonable time. It is generally considered that several simultaneous mechanisms contribute to densification during HP. As well as diffusion, enhanced by the applied pressure, grain boundary sliding and plastic flow have some effect. With a liquid phase present, the applied pressure is thought to be merely additive to the capillary pressure (Kingery *et al.*, 1963).

3.3.2 HIP

HIP combines high temperature (up to 2200°C) and a gas pressure (200–500 MPa), which is uniformly applied to the powder compact in all directions, usually through an impermeable membrane to encapsulate the ceramic component. An almost fully densified body with no open porosity can also be hot-isostatically pressed directly without encapsulation. This technique allows theoretical density to be reached at lower temperatures than by pressureless sintering with limited grain growth.

3.3.3 SPS

SPS (Nygren and Shen, 2003), also known as FAST, uses an electrical current (DC, pulsed DC, or AC) which is passed through a conducting pressure die (graphite) and, if the material has reasonable electrical conductivity, through the ceramic itself. The die therefore acts as a heat source, so the sample is heated both internally and externally. Contrary to HIP, the SPS technique allows very rapid heating and cooling rates, very short holding times (a few minutes) and results in densification at much lower sintering temperatures, usually a few hundred degrees lower than for conventional sintering with restricted grain growth occurring only at the last sintering stage as shown in **Fig. 30**.

3.3.4 Flash sintering

This method is also referred to as the "two-electrode experiment" by Raj *et al.* (2011) and the process consists in heating the ceramic piece in a conventional furnace but applying an electrical current (DC or AC). The green sample is hung in the middle of the kiln by two platinum electrodes allowing the passage of current. At low fields (less than 40 V cm^{-1}), the sintering rate increase is attributed to a reduction of the grain growth under an applied field; at higher fields, the specimens sinter almost instantaneously, as if in a flash, above a critical temperature (Cologna *et al.*, 2010). Several oxides have been sintered using this technique such as cobalt-manganese spinel, MgO-doped alumina, cubic and tetragonal zirconia but the fundamental mechanism of the very rapid mass transport involved remains obscure.

Fig. 31 shows the shrinkage strain in yttria stabilized tetragonal zirconia powder compacts with four different particle sizes at 0 and 100 V cm^{-1}, measured as the furnace is ramped up at a constant heating rate of 10°C min^{-1}. Without electric field, the samples sinter slowly as the temperature rises and the sintering rate is most rapid for the smallest particle size specimen. The application of an electric field (100 V cm^{-1}) results in nearly instantaneous sintering. The threshold temperature for the onset of flash sintering moves lower as the particle size decreases.

The comparison of 1 μm conventionally and flash sintered samples (**Fig. 32**) shows that grains of less than 100 nm are more heavily populated in the flash sintering specimen.

3.4 Composition Modification

3.4.1 Addition of dopant elements to modify grain boundary energy

Dopants can be introduced to modify grain boundary energy. When the concentration of the dopant is greater than the solubility limit in the major component, then segregation occurs at grain boundaries (region II in **Fig. 33**). Grain boundary mobility is

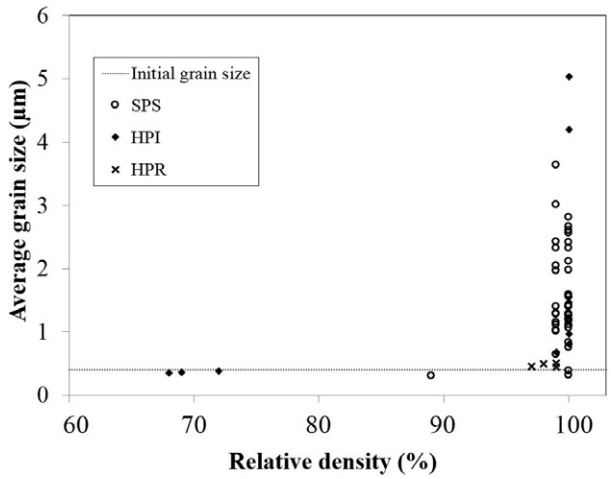

Fig. 30 Alumina grain size vs. density for specimens sintered by spark plasma sintering (SPS), hot pressing under resistive heating conditions (HPR) and hot pressing under inductive heating conditions (HPI) techniques (Demuynck, 2011).

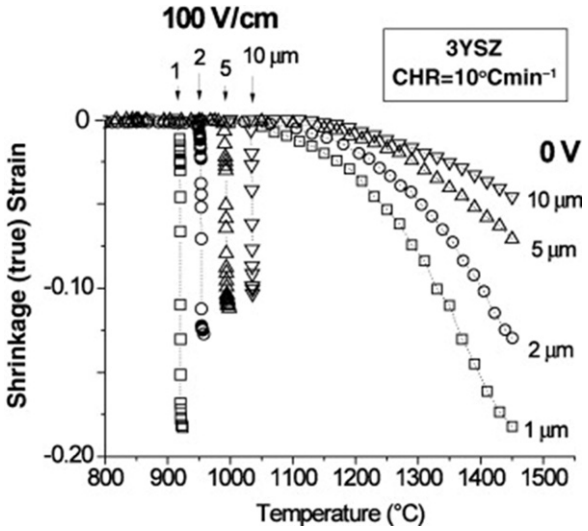

Fig. 31 Activated/assisted sintering of commercial yttria stabilized tetragonal zirconia powder (Francis *et al.*, 2012).

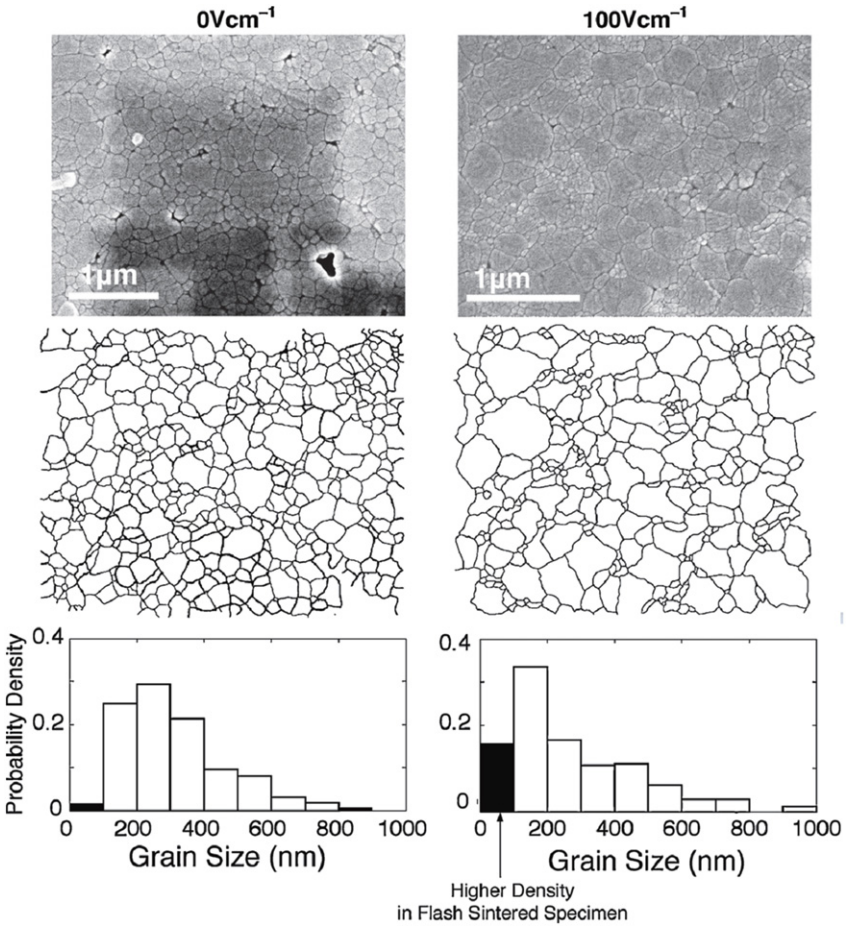

Fig. 32 Micrographs of 1 µm conventionally and flash sintered samples (Francis *et al.*, 2012).

slowed by segregated dopant ions. Concentration of maximum dopant increases with surface to volume ratio of the grain, i.e., it is higher for nanosize grains. Above a given concentration, a new (dopant-rich) phase precipitates. Precipitation occurs at lower dopant concentrations as grain size increases. (region III in **Fig. 33**).

Figs. 33 and 34 show some examples of grain growth slow down for alumina doped with yttria and magnesia. Fig. 35 presents an example of combined effects of using the SPS technique and yttria doping on a zirconia ceramic which allows a nanosized microstructure to be maintained.

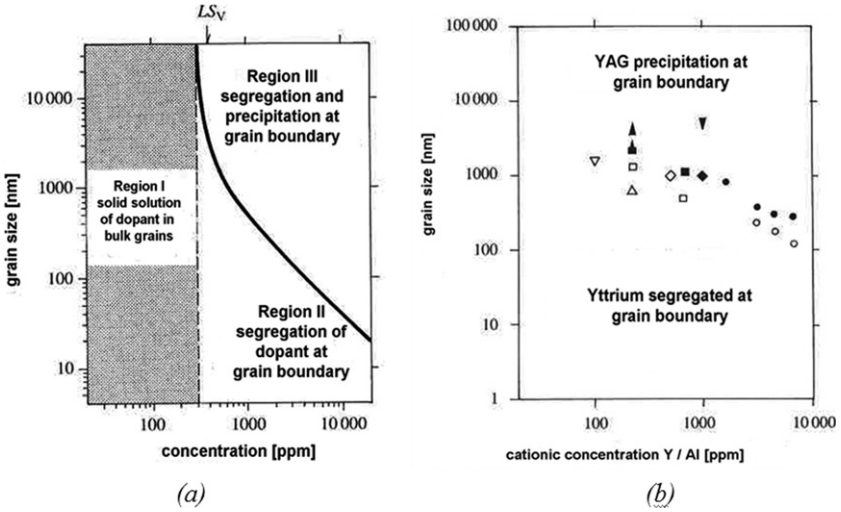

Fig. 33 (a) Grain boundary segregation-precipitation for doped polycrystal vs. grain size and dopant content. (b) Example of segregation of Y^{3+} at alumina grain boundaries (Haussonne *et al.*, 2005).

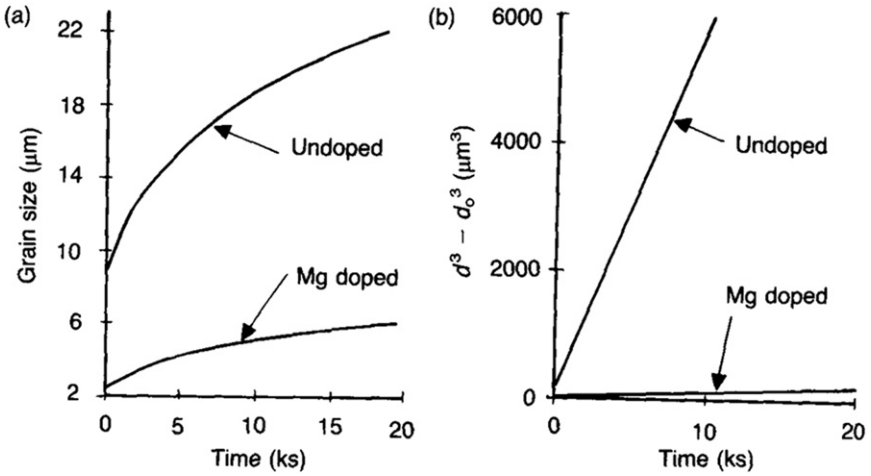

Fig. 34 Grain growth kinetic for pure alumina and MgO doped alumina (Lee and Rainforth, 1994).

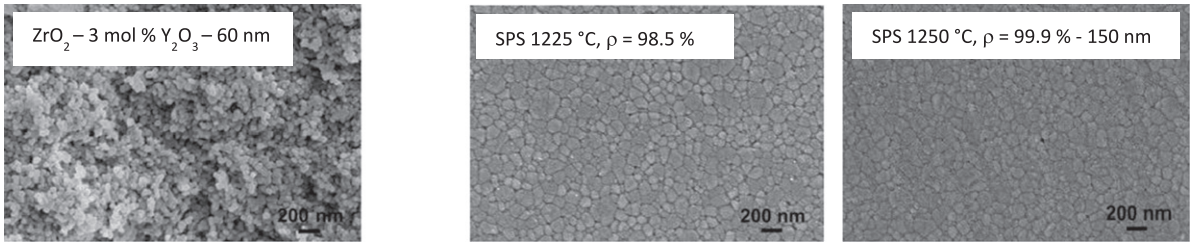

Fig. 35 Grain growth during spark plasma sintering (SPS) of zirconia: (a) initial powder, (b) sintered ceramics (Reddy *et al.*, 2010).

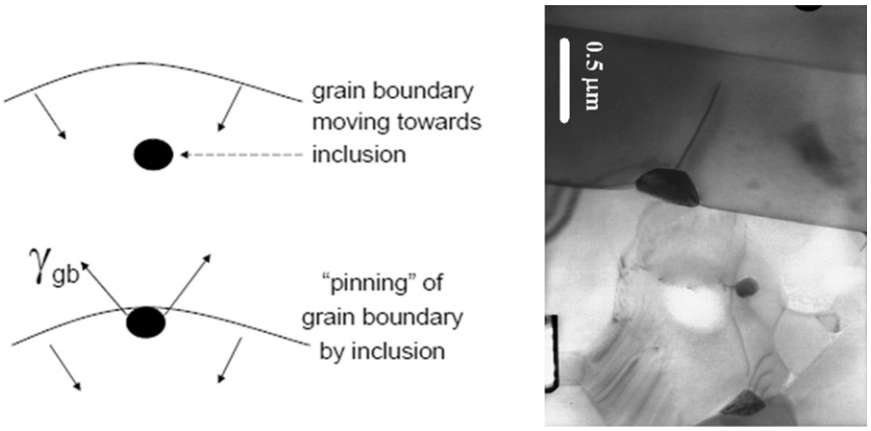

Fig. 36 Schematic illustration of effect of inclusion on grain boundary mobility (Petit, 2002).

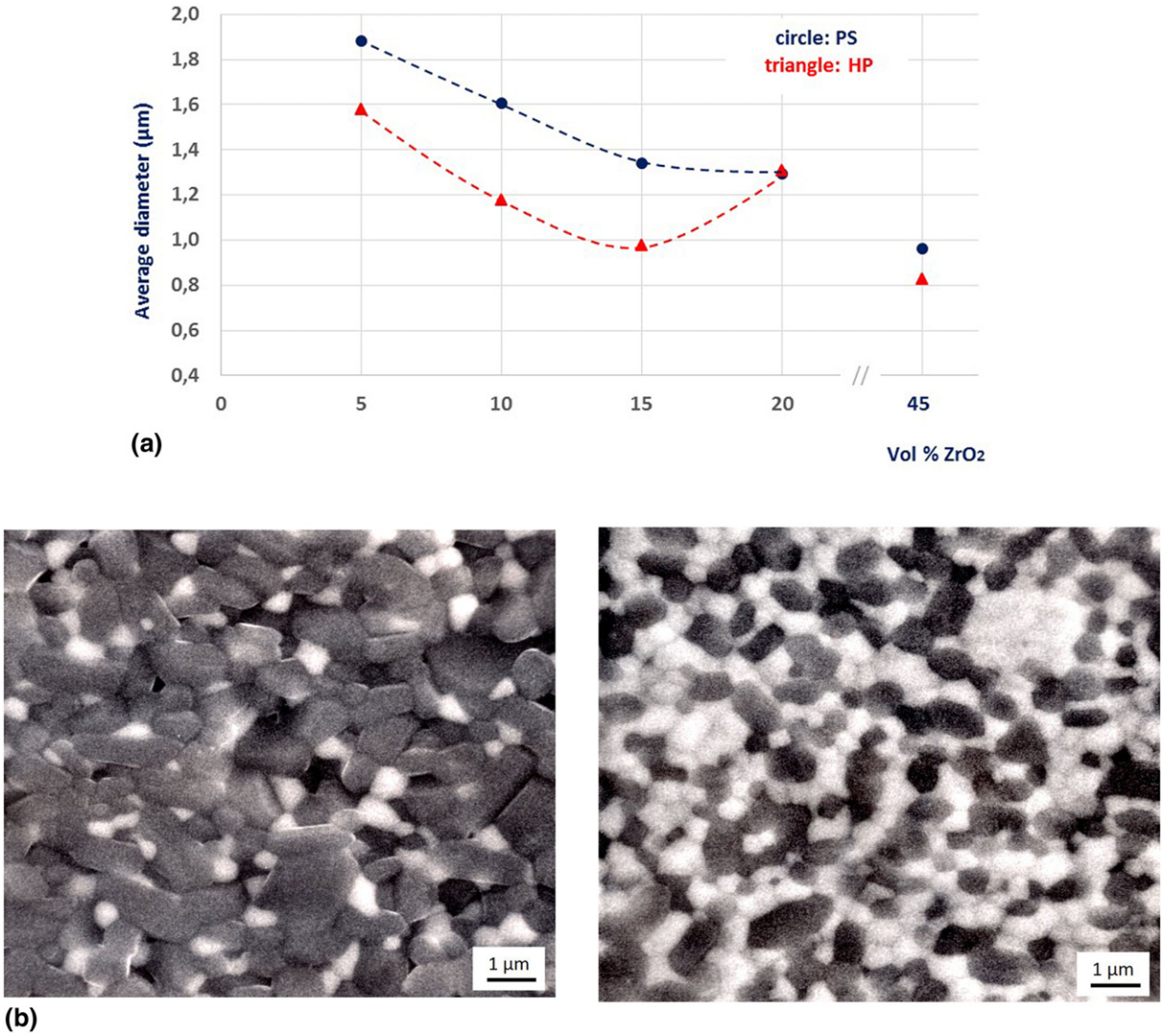

Fig. 37 (a) Decrease of matrix grain size with zirconia content for zirconia toughened alumina composites densified by hot pressing (HP) and pressureless sintering (PS), (b) microstructures of composites containing 15 and 45 vol% of zirconia (Leriche *et al.*, 1988).

3.4.2 Addition of extra small particles at grain boundaries

3.4.2.1 First example

If insoluble particles are dispersed in a ceramic matrix, grain growth will be slowed down (or even stopped). Inclusions will exert blocking forces opposed to grain boundary mobility, resulting in so-called "pinning" of grain boundaries as shown in **Fig. 36**. The blocking force is equal to the grain boundary migration force for a given grain size d (Zener equation: see also Manohar *et al.*, 1998):

$$d_{\max} = \alpha 2 r_i / f_i \tag{19}$$

where r_i is the inclusion particle radius and f_i is the volume fraction of inclusions. This Eq. (19) demonstrates that grain growth will depend on the inclusion size, which must be lower than the desired grain size, and on inclusion content.

Fig. 37 shows the influence of insoluble particle content (zirconia) on matrix grain growth (alumina grains) for zirconia toughened alumina composites.

Fig. 38 shows the influence of insoluble particle content (nanosized silicon carbide) on matrix grain growth (alumina grains) for alumina–silicon carbide nanocomposites. The addition of only 1 vol% of nanometric silicon carbide into an alumina matrix allows the reduction of the matrix grain size and induces a fracture mode change from intergranular to transgranular.

Moreover, if the expansion coefficient of dispersed particles is inferior to the matrix coefficient, the dislocations can move under traction matrix and form a substructure inside the matrix grains as shown in **Fig. 39** and a refinement of the matrix with a resulting increase of flexural strength as shown in **Fig. 40**.

3.4.2.2 Second example

If the inclusions are slightly soluble in the matrix then Ostwald ripening may occur leading to a decrease in the number of small particles and growth of larger ones. According to Laplace's law, the atoms of a particle close to the inclusion–matrix interface are

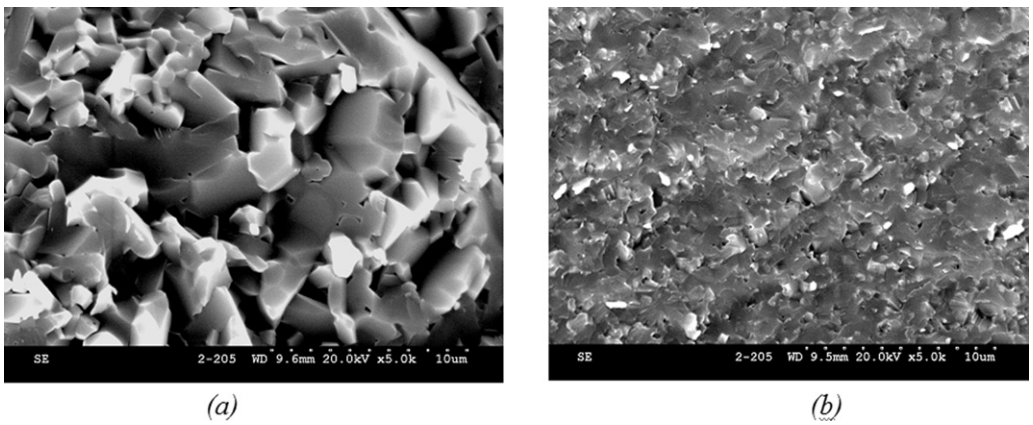

Fig. 38 Micrographs of (a) pure alumina grit fracture faces, (b) alumina + 1 vol% SiC grit fracture face (Kermel, 2003).

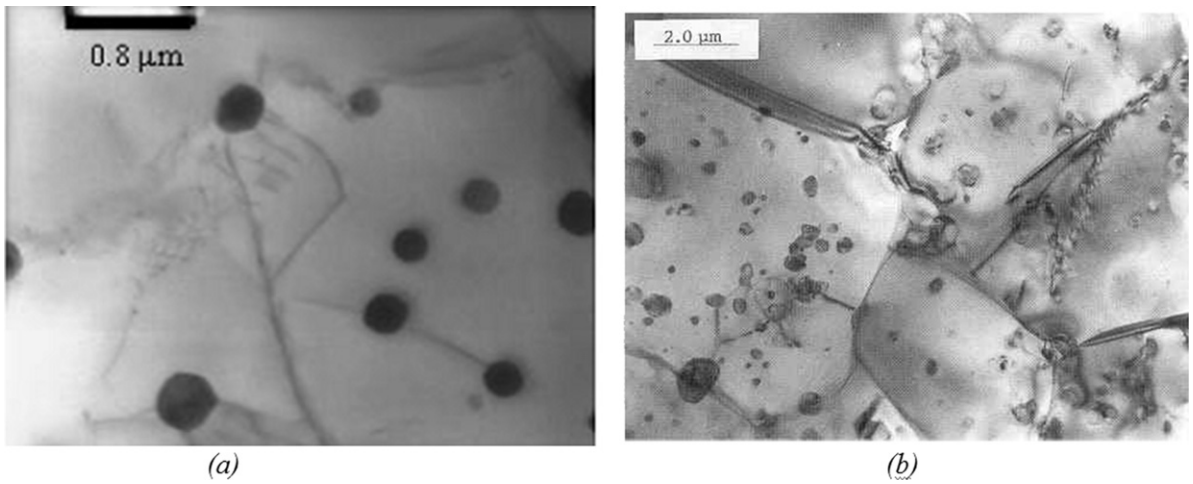

Fig. 39 Substructure forming by dislocation movement: (a) alumina/nanometric Mo particles (Petit, 2002), (b) alumina/nanometric SiC particles (O'Sullivan, 1997).

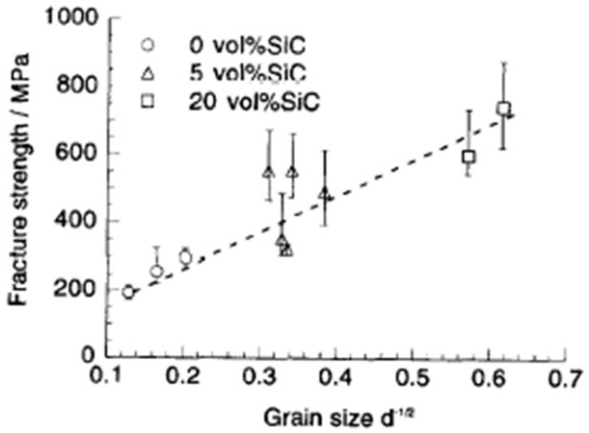

Fig. 40 Flexural strength increase of SiC particle reinforced TZP with decrease in matrix grain size (Bamba *et al.*, 1998).

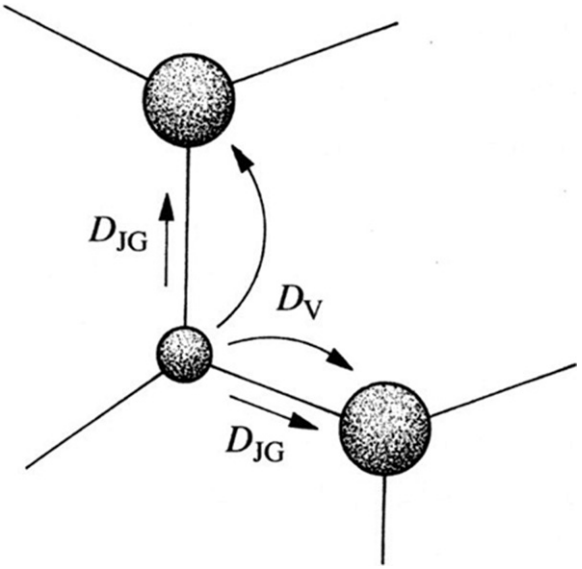

Fig. 41 Grain growth by Ostwald ripening (Haussonne *et al.*, 2005).

submitted to compressive forces (as large as the inclusion is small). The chemical potential of these atoms increases which enhances their solubility in the matrix resulting in a flow of atoms from small particles toward larger ones through a dissolution – diffusion – precipitation mechanism (**Fig. 41**).

4 Summary

Fabrication of ceramics includes a heat treatment of a powder compact to form a dense solid. This process of sintering involves matter transport to reduce porosity by diffusion of atoms in the vapor phase, in the liquid phase or in the solid state. Most mechanisms are activated thermally in order to overcome the potential barrier between the initial state of higher energy (porous powder compact) and the final state of lower energy (consolidated dense material). The chapter has outlined the processes involved in solid state sintering in the absence of any liquid phase and liquid phase sintering in the presence of a small volume percent of liquid phase. In all cases, the driving force for densification lies in the reduction of the surface energy resulting from the reduction in the interfacial area between gas and liquid/solid phases.

In all cases, simultaneously with the densification phenomenon, grain growth occurs which influences the final microstructure. So, it is crucial to know the impact of all process parameters on grain growth and densification mechanisms in order to control the final ceramic microstructure and the resulting properties.

The methods to control the microstructure of ceramics depend on the product. Ceramic materials with 97–98% densification level and normal grain growth can be processed by pressureless sintering with appropriate thermal treatment conditions (temperature, duration) in order to favor lattice or grain boundary atom diffusion favorable to densification and to limit the

surface diffusion responsible for grain growth. For systems which are susceptible to EGG, it is necessary to use special thermal regimes or schedules such as "fast firing," "controlled rate sintering," or "microwave sintering" or to add very small amounts of other chemical species (grain growth inhibitors, submicron particles) in order to limit the grain growth by decreasing the grain boundary mobility. For liquid phase sintered ceramics, the microstructure can be controlled by adapting the intergranular phase viscosity and the seed content.

Fully dense ceramic materials with limited grain growth can be obtained by applying new technologies adding supplementary effects (application of external pressure and/or electric current) to fine grain size and well-dispersed powders. Moreover, these new techniques allow decrease of temperature and the duration of sintering and so are particularly promising for potential energy savings.

References

Bamba, N., Choa, Y., Sekino, T., Niihara, K., 1998. Microstructure and mechanical properties of yttria stabilized zirconia-silicon carbide nanocomposites. Journal of the European Ceramic Society 18, 693–699.

Barsoum, M.W., 2002. Fundamentals of Ceramics. Oxford: Taylor and Francis.

Binner, J., Vaidhyanathan, B., 2008. Processing of bulk nanostructured ceramics. Journal of the European Ceramic Society 28 (7), 1329–1339.

Brook, R.J., 1969. Pore – grain boundary interactions and grain growth. Journal of American Ceramic Society 52, 56–57.

Brosnan, K.H., Messing, G.L., Agrawal, D.K., 2003. Microwave sintering of alumina at 2.45 GHz. Journal of the American Ceramic Society 86 (8), 1307–1312.

Cologna, M., Rashkova, B., Raj, R., 2010. Flash sintering of nanograin zirconia in <5 s at 850°C. Journal of the American Ceramic Society 93 (11), 3556–3559.

Demuynck, M., 2011. Spark plasma sintering (SPS). Evaluation critique d'une methode de frittage rapide et de son applicabilité aux céramiques techniques et composites. PhD thesis, Université Catholique de Louvain, Belgium.

Ewsuk, K.G., Messing, G.L., 1989. A theoretical and experimental analysis of final-stage densification of alumina during hot isostatic pressing. In: Schaefer, R.J., Linzer, M. (Eds.), Proceedings of the 2nd International Conference on HIP: Theory and Applications, pp. 23–33. Ohio: ASM International.

Francis, J.S.C., Cologna, M., Raj, R., 2012. Particle size effects in flash sintering. Journal of the European Ceramic Society 32, 3129–3136.

Hampshire, S., 2014. Fundamental aspects of hard ceramics. Chapter 1. In: Llanes, L., Mari, D. (Eds.), Comprehensive Hard Materials, Volume 2: Ceramics. London: Elsevier, pp. 3–28. (Editor-in-Chief: Sarin, V.K.).

Hampshire, S., Pomeroy, M.J., 2012. Grain boundary glasses in silicon nitride: A review of chemistry, properties and crystallisation. Journal of the European Ceramic Society 32, 1925–1932.

Harmer, M.P., Brook, R.J., 1981. Fast firing – Microstructural benefits. Transactions and Journal of the British Ceramic Society 80, 147–149.

Haussonne, J.M., Carry, C., Bowen, P., Barton, J., 2005. Céramiques et Verres. Principes et techniques d'élaboration. In: Traité des Matériaux, vol. 16. Lausanne: Presses Polytechniques et Universitaires Romandes.

Herring, C., 1951. Surface tension as a motivation for sintering. In: Kington, W.E. (Ed.), The Physics of Powder Metallurgy. New York, NY: McGraw-Hill, pp. 143–179.

Jackson, B., Ford, W.F., White, J., 1963. The influence of Cr_2O_3 and Fe_2O_3 on the wetting of periclase grains by liquid silicate. Transactions and Journal of the British Ceramic Society 62, 577–601.

Kang, S.-J.L., 2005. Sintering, Densification, Grain Growth and Microstructure. Oxford: Elsevier Butterworth-Heinemann.

Kingery, W.D., 1959. Sintering in the presence of a liquid phase. Journal of Applied Physics 30, 301–306.

Kingery, W.D., Bowen, H.K., Uhlmann, D.R., 1976. Introduction to Ceramics, second ed. New York, NY: Wiley.

Kingery, W.D., Woulbroun, J.M., Charvat, F.R., 1963. Effects of applied pressure on densification during sintering in the presence of a liquid phase. Journal of the American Ceramic Society 46, 391–395.

Kuczynski, G.C., 1949. Self-diffusion in sintering of metallic particles. Journal of Metals 1, 169–178.

Lee, W.E., Rainforth, W.M., 1994. Ceramic Microstructures: Property Control by Processing. London: Chapman & Hall.

Leriche, A., 1986. Influence des paramètes d'élaboration de composite mullite-zircone sur leur microstructure. PhD thesis, Université de Mons, Belgium.

Leriche, A., Moortgat, G., Cambier, F., *et al.*, 1988. Preparation and microstructure of zirconia-toughened alumina ceramics. In: Somiya, S., Yamamoto, N., Yanagida, H. (Eds.), Advances in Ceramics 24. Westerville, OH: American Ceramic Society. Science and Technology of Zirconia III.

Manohar, P.A., Ferry, M., Chandra, T., 1998. Five decades of the Zener equation. ISIJ International 38 (9), 913–924.

Nygren, M., Shen, Z., 2003. On the preparation of bio-, nano- and structural ceramics and composites by spark plasma sintering. Solid State Sciences 5, 125–131.

O'Sullivan D., 1997. Fabrication and mechanical characterization of alumina-silicon carbide nanocomposites. PhD thesis, Université de Valenciennes et du Hainaut Cambrésis, France.

Palmour III, H., Huckabee, M.L., Hare, T.M., 1977. Rate controlled sintering, principles and practice. In: Ristic, M.M. (Ed.), Proceedings of the 4th Round Table Conference on Sintering: New Developments, pp. 46–66. Dubrovnik. Amsterdam: Elsevier.

Palmour III, H., Johnson, D.R., 1967. Phenomenological model for rate-controlled sintering. In: Kuczynski, G.C., Hooton, N.A., Gibbon, C.F. (Eds.), Sintering and Related Phenomena. New York, NY: Gordon & Breach, pp. 779–791.

Petit, F., 2002. Synthèse et propriétés de composites à matrice céramique renforcée par du métal. PhD Thesis, Université de Valenciennes, France.

Rahaman, M.N., 1995. Ceramic Processing and Sintering. New York, NY: Marcel Dekker, Inc.

Rahaman, M.N., 2003. Ceramic Processing and Sintering, second ed. Boca Raton, FL: CRC Press – Taylor and Francis.

Raj, R., Chyung, C.K., 1980. Solution-precipitation creep in glass ceramics. Acta Metallurgica 29, 159–166.

Raj, R., Cologna, M., Francis, J.S.C., 2011. Influence of externally imposed and internally generated electrical fields on grain growth, diffusional creep, sintering and related phenomena in ceramics. Journal of the American Ceramic Society 94 (7), 1941–1965.

Reddy, K.M., Kumar, N., Basu, B., 2010. Inhibition of grain growth during the final stage of multi-stage spark plasma sintering of oxide ceramics. Scripta Materialia 63, 585–588.

Smith, C.S., 1948. Grains, phases and interfaces – An interpretation of microstructure. Transactions of AIME. 175, 15–51.